Research Square

Preprints are preliminary reports that have not undergone peer review.
They should not be considered conclusive, used to inform clinical practice,
or referenced by the media as validated information.

Experimental Stone Walls for Heritage Research: Investigating Spatial Moisture Patterns Using ERT and Microwave Sensing

Oliver Sass

oliver.sass@uni-bayreuth.de

University of Bayreuth

Alireza Madani

University of Bayreuth

Article

Keywords:

Posted Date: November 25th, 2026

DOI: https://doi.org/10.21203/rs.3.rs-11514637/v1

License: This work is licensed under a Creative Commons Attribution 4.0 International License.
Read Full License

Additional Declarations: No competing interests reported.

Experimental Stone Walls for Heritage Research: Investigating Spatial Moisture Patterns Using ERT and Microwave Sensing

Oliver Sass[a,*] and Alireza Madani[a]

[a] Faculty of Biology, Chemistry & Earth Sciences, Chair of Geomorphology, University of Bayreuth, Bayreuth, Germany

* Corresponding author: Oliver Sass (oliver.sass@uni-bayreuth.de)

E-mail: alireza.madani@uni-bayreuth.de (Alireza Madani)

Abstract

Moisture contributes to historic stone-masonry deterioration, yet spatial assessment is difficult because of heterogeneous materials, uncertain structures and restrictions on invasive measurements. Two full-scale outdoor test walls with documented construction compare Trebgast sandstone under contrasting hydrological conditions: uncovered, sand-filled ROCK and roofed, drained, ventilated HOUSE. Eight campaigns in 2022–2023 used electrical resistivity tomography (ERT) and handheld microwave (MW) sensing. ROCK was generally wetter than HOUSE, especially toward the inner wall side and base, consistent with backfill supply, top infiltration and basal capillary rise. Wall orientation was secondary: Moisture levels at ROCK followed the order N>W>E>S, whereas HOUSE showed a less pronounced pattern. ERT–MW covariation was moderate at shallow depth and strong at deeper sampling depth, the latter largely reflecting the ROCK–HOUSE contrast. Our test wall approach supports the interpretation of hydrological controls and complementary spatial sensitivities while transfer to heritage sites requires material-specific calibration and field validation.

1. Introduction

Water plays a fundamental role in rock weathering as well as in the deterioration of built heritage [1], where "moisture is the main cause or concause of decay" [2, p. 1372]. Rock moisture is fundamentally important for almost all weathering processes, e.g. for frost cracking [3,4,5], salt weathering [6,7] or long-term subcritical cracking [8]. Different scales and processes have to be considered for weathering studies and risk assessment. While chemical weathering and biological activity generally increase with moisture availability and time of wetness [9,10], salt weathering is often exacerbated by repeated moisture fluctuations around crystallization/dissolution thresholds [11]. Ongoing climate change is expected to alter the patterns and fluctuations of moisture in stonework and thereby modify stone-decay processes e.g. [12,13]. This makes building stone a "large scale laboratory" in which the impact of environmental drivers on weathering conditions in past and future can be studied [14].

However, quantitative knowledge about material moisture in natural or built environments remains more limited than temperature records, partly because robust moisture measurements are difficult to obtain [1,15–18]. Buildings, rock-hewn sites and rockwalls all present hydrological complexities [1,19] and moisture availability may strongly differ on small scales. Furthermore, vegetation can modify the near-surface microclimate around historic masonry [20]. Understanding such small-scale moisture distribution is complicated by the lack of universally reliable sensors. Numerous reviews and comparative evaluations of different moisture measurement techniques in stone are available [16,17,21], showing that no single method is suitable for all materials and questions. The complex heterogeneity of stonework or rock in terms of microclimate, microtopography, different stone types, etc. would require a high number of monitoring sensors, which is often not possible because of financial, technical and monument-protection constraints. The internal structure of stonework in terms of pore volume, crack patterns, mortar or reinforcements is often unknown, which complicates interpretation [1,16].

To address these methodological and interpretative challenges, full-scale experimental walls can provide a complementary research setting between laboratory specimens and historic buildings. Their geometry, stone types and construction details can be documented, while outdoor exposure and fixed measurement positions permit repeated observations. Unlike a real monument, such a testbed can also accommodate more extensive instrumentation and controlled wetting experiments. It does not reproduce the full complexity of any one historic structure, but allows typical, generalized moisture patterns to be investigated. Similar artificial masonry experiments have been used to examine rising damp [18,19]. The UBT experiment applies this experimental approach to natural stone and contrasts free-standing wall and building-like boundary conditions. The present paper addresses three questions: (i) how do these contrasting structural configurations relate to spatial moisture patterns in the same sandstone; (ii) how do orientation, wall position and depth modify these patterns; and (iii) what complementary information do ERT and MW provide? The wider ten-year programme also targets longer-term objectives like event-scale responses, temporal dynamics, weathering, establishing biota and future calibration (Table 1).

The specific contribution of the present analysis is to examine spatial moisture distribution across two documented, full-scale outdoor configurations using two non-destructive moisture sensing techniques. This comparison provides a controlled-material reference for identifying which observed moisture contrasts are associated with the overall construction and exposure configuration, and which vary with measurement geometry. This distinction is relevant when interpreting moisture surveys of heritage stonework, where construction details and subsurface conditions may be incompletely known.

Table 1. Aims and research questions of the long-term testwall programme

Research theme	Questions and aims
Spatial distribution of moisture (how does water enter the structure?)	• Importance of capillary rise? • Importance of radiation and wind-driven rain? • Water penetration through cracks or mortar joints, resp.? • Importance of water infiltration from top (horizontal rainfall)? • Importance of exchange with interior (deeper rock / indoor air)?
Temporal distribution of moisture	• Reaction on rainfall? • Seasonal distribution?
Weathering and biota	• Which types of weathering occur after 2, 5, 10 yrs? • Spatial correlation to moisture level and fluctuations? • Which plants and lichen colonise the stone? • Are lichen and mosses increasing or decreasing wetness? • Are climbing plants (e.g. ivy) increasing or decreasing wetness?
Methodological questions	• Pre-testing measurement equipment before applying at field sites • Calibration of different methods (laboratory and field sprinkler tests) • Which methods are advisable? • How do different methods correlate? • How do measurement and modeling results correlate?

2. Methods

Two cube-shaped experimental structures (hereafter “cubes”) were built at the University of Bayreuth to examine natural-stone moisture under contrasting, documented configurations. The approximately 2 × 2 m structures are referred to as ROCK, an uncovered rock-outcrop or ruin analogue, and HOUSE, a roofed building analogue. Both are constructed from 30 × 30 × 30 cm natural-stone blocks. The structures are research analogues rather than replicas of any specific historic monument; their relevance to built heritage lies in isolating observable moisture-pattern contrasts under well-described construction conditions.

Both cubes are aligned with the cardinal directions, resulting in defined north, west, south, and east faces. In the corners, concrete columns were erected to give the structures stability (Fig. 1). Both cubes were built on a former hydrogeological test site consisting of two concrete basins filled with sand. For erecting the cubes the basins were emptied, strip foundations were laid and the sand was refilled.

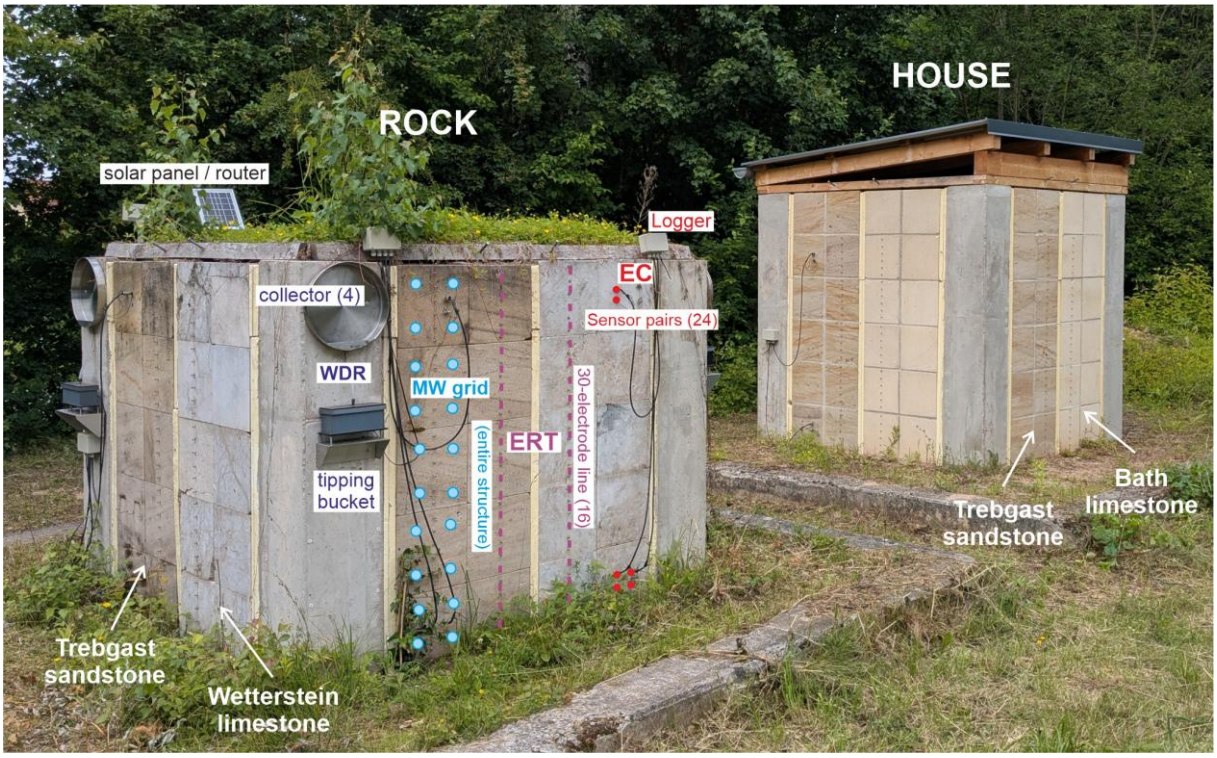


Fig. 1: UBT Testwalls ("cubes") on 15th June 2026; instrumentation highlighted. Photo: A. Mitchell.

ROCK is intended to represent a natural rock structure or free-standing wall. It is 1.5 m high (five rows of 30 cm stone blocks) and the structure is uncovered on the top. The blocks were stacked on top of each other without mortar using dry construction methods; special adhesive was applied to the innermost (furthest from the wall surface) approx. 10 cm of the contact surfaces to ensure stability. The space between the four walls was backfilled with sand which allows rainwater to infiltrate (and potentially, to infiltrate the stones from their back sides). This setup was chosen to simulate wet interior conditions with a supposed moisture gradient from inside to outside. The upper edge of the strip foundation is slightly lower than the sand fill of the basin, so that the lower 5 cm of the stones are sitting in the sand allowing capillary rise to occur.

In contrast, HOUSE is 1.8 m high (six rows of stone) and has a simple pent roof; rainwater runoff is drained away via rain gutters and seeps into the ground away from the basins. The blocks were laid using a traditional lime mortar. The inside of the structure is accessible through a small door (taking up the space of two stone columns at the east face); it is unheated and

well ventilated through a gap between the roof and masonry. The upper edge of the strip foundation is a few cm above the sand surface, which hampers capillary rise.

Both cubes are made of two different types of stone, in such a way that each wall consists of two separate parts. At both cubes we used Trebgast Sandstone, which sometimes forms small outcrops and escarpments in Upper Franconia, and which has been frequently used in construction at historic buildings in and around Bayreuth. At ROCK we additionally used Wetterstein limestone, a light-gray, low-porosity limestone that builds up large areas of the German and Austrian Calcareous Alps including Germany's highest mountain, the Zugspitze. At HOUSE, the second stone type is Bath Limestone, a light-coloured arenic limestone which was used in the construction of numerous historic buildings in Oxford (UK); that was to establish a connection with the working group of Oxford Resilient Buildings and Landscapes Lab (OxRBL). All three types of stones were ordered at quarries in Upper Franconia, Upper Bavaria and England, respectively, and delivered to Bayreuth. When placing the order, we requested that the stones originate from a contiguous area of the quarry in order to keep the rock parameters as similar as possible. Each stone cube was photographed from all six sides before installation. The respective rock properties are summarised in Table 2.

Table 2: Description of the stone types used for testwall construction

	Trebgast sandstone	**Wetterstein limestone**	**Bath limestone**
description	medium-grained quartz sandstone with siliceous cementation	micritic to sparitic limestone	fine grained oolitic limestone
composition	quartz (76%), alkali feldspar (14%), rock fragments (9%)[1]	97 – 99% $CaCO_3$	predominantly calcite, with minor clay minerals and iron minerals[2]
porosity	18 – 20% (intergranular)	0.5 – 1.0% (cracks and micro-fissures)	20 – 24% (intergranular)
density	2,100 kg m^{-3}	2,600 kg m^{-3}	2,060 kg m^{-3}
quarry	Bamberger Natursteinwerke 50°02'57"N, 11°33'19"E	Stadler, Fischbach am Inn 47°42'20"N, 12°08'33"E	Hartham Park, Lovell Stones Group 51°25'51"N, 2°12'34"W

1: according to quarry company (Bamberger Natursteinwerke)

2: according to Tucker & Fosbury [22]

2.1 Relevance of the experimental design to built heritage

The HOUSE structure shares selected features with historic stone masonry, including natural-stone units and lime-mortar joints, while the ROCK structure represents exposed, uncovered stonework with earth contact and a moisture-supplying interior. They represent different combinations of water supply, drainage, cover, ventilation and joint construction. Consequently, differences between the structures can be linked to the combined boundary-condition configuration, but the individual contribution of each factor cannot be quantified from this comparison alone. The documented geometry and repeatable access provide a reference for assessing non-destructive sensing methods before extending interpretations to heterogeneous heritage masonry. Using Trebgast sandstone in both structures provides a shared material basis for the ROCK–HOUSE comparison.

2.2 Climate of the site

Meteorological conditions were monitored by a weather station installed directly adjacent to the experimental structures. The available 2022–2023 records were evaluated at hourly resolution. A wind-driven-rain (WDR) exposure index was derived from coincident rainfall, wind speed and wind direction using the windward component for each façade azimuth. Solar radiation was measured directly by the weather station. For each measurement timestamp, solar azimuth was derived from the local date and time and the geographic coordinates of the test-wall site (49.930215° N, 11.579620° E) [23]. To emphasize directional contrasts, WDR and solar radiation distributions in Fig. 2 are expressed relative to the maximum value of the respective panel.

The resulting directional forcing is strongly asymmetric. WDR exposure is concentrated in the western sector, with the maximum in the WSW–W range and almost equally high exposure for the due west-facing surface. In contrast, measured solar radiation is concentrated in the southern sector of the solar path, while northern solar azimuths are absent. Thus, the site combines WDR exposure from the west with predominantly southern solar forcing.

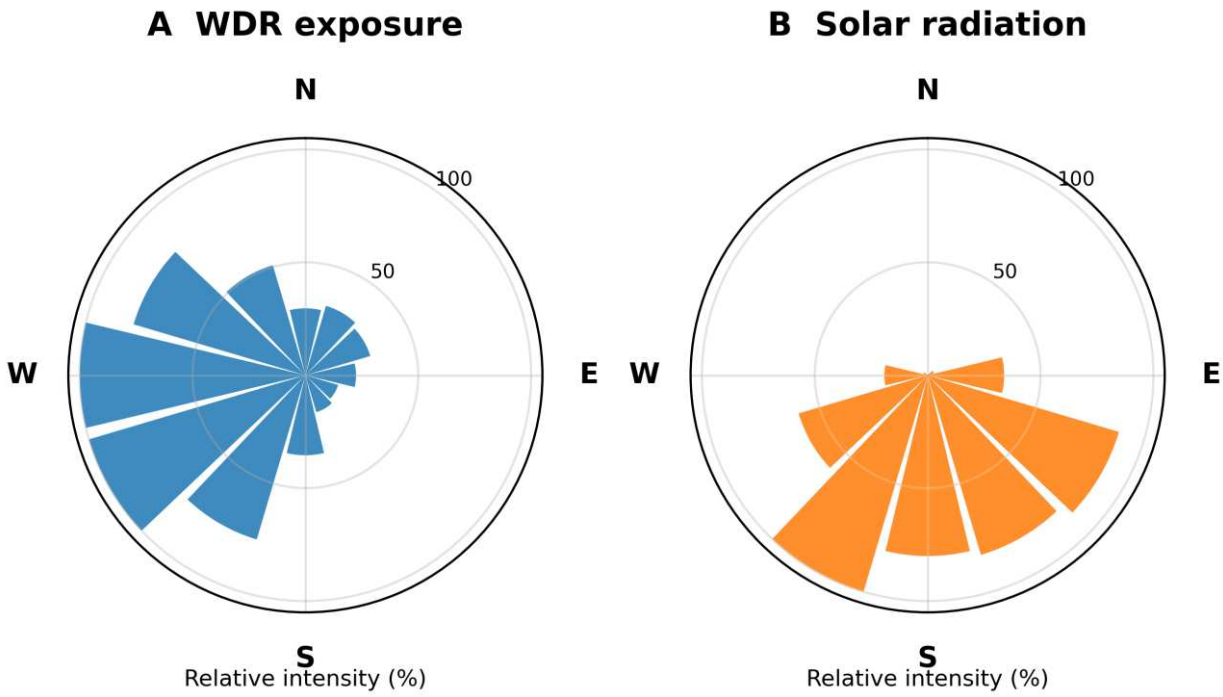


Fig. 2: Relative directional meteorological forcing at the UBT test wall site during 2022–2023. (A) Wind-driven-rain (WDR) exposure derived from coincident hourly rainfall, wind speed and wind direction, including the windward component for each façade azimuth. (B) Measured solar radiation grouped by solar azimuth derived from the measurement timestamp and the test-site coordinates (49.930215° N, 11.579620° E). Values in each panel are normalized to the respective maximum (= 100%).

2.3 Instrumentation

The measurement concept comprises continuous and monthly measurements. All applied techniques and their basic measurement parameters are summarized in Table 3. In this paper we focus on the spatial distribution of stone moisture by evaluating 2D-geoelectrics and microwave handheld sensor data from the years 2022 and 2023. Only these two methods will be described in more detail below.

Table 3. Test-wall instrumentation and monitoring concept. X: Measurement methods explained in more detail in the text.

Measurement	Details
Continuous measurements	
Electrical resistance	two-point transitional resistivity, combined with temperature sensors, self-built data loggers with automatic data transmission and storage, eight loggers with three sensor pairs each; interval 10 mins
Microwave monitoring	microwave reflectance, hf-sensor types PM (0-7 cm) and RM (0-13 cm), storage at central datalogger, interval 10 mins (two years only)
Meteorological station	(HOBO), including air temperature, air humidity, wind speed, wind direction and radiation, interval 10 mins
Groundwater level	within ROCK basin and within ROCK cube, pressure sensor, Solinst Levellogger, interval 1 hr
Monthly measurements	
2D-geoelectrics (ERT) **(X)**	GeoTom (Geolog2000) with self-manufactured cable tree, 16 vertical profiles with 30 electrodes each
Microwave handheld sensors **(X)**	microwave reflectance, hf-sensor types R1M (0-3 cm) and PM (0-25 cm), rectangular grid with four measurement points on each stone block
Infrared thermography	OPTRIS IR-Camera, all eight faces (discontinuously for technical reasons)
Photo documentation	normal optical (RGB) photos, 16 megapixel, all eight faces

In 2D-resistivity (ERT) measurements, a constant current is fed into the ground at two electrodes and the voltage generated is measured at two further electrodes. By combining numerous measurements along a profile line, a 2D-profile of the resistance distribution in the subsurface is generated, which usually correlates with the water content. At the UBT testwall, ERT measurements are regularly carried out using a GeoTom device, manufacturer Geolog2000, Augsburg, Germany. Each profile line runs vertically along one column of stones (2 cubes x 4 directions x 2 stone types = 16 profiles). Each profile consists of 30 electrodes at a spacing of 5 cm (six electrodes in each of the five stones), which results in a profile length of 1.45 m. Small hexagonal machine screws that are screwed into metal plugs (1 cm deep drillholes, 5 mm wide) are used as electrodes; the spread metal plugs ensure tight and reliable electrical contact to the stone. Measurements are carried out using a hand-manufactured cable tree which is connected to the screws by crocodile clips. To prevent the electric field from being influenced by neighbouring stone types or concrete pillars, the different wall sections are separated from each other by insulating foam boards. For more details on ERT measurements and their application on stone we refer to Sass & Viles [24], Rode et al. [25] and Sass & Heil [26].

Microwave handheld sensors (MW) are based on microwave reflectance, which is strongly influenced by pore saturation of the medium under investigation. We use the device MOIST 350B manufactured by hf-sensor (Leipzig, Germany), equipped with different handheld sensors; we regularly use the types R1M (penetration depth 0–3 cm) and PM (0–25 cm).

Measurements are carried out in a rectangular grid with four measurement points (arranged like the '4' on a dice) on each stone block (cf. Fig. 1). This amounts to 320 measurement points at ROCK and 336 points at HOUSE for each sensor. Without stone-specific calibration, the MOIST 350B outputs a dimensionless moisture index (MI). Published calibration studies show that microwave response is strongly related to water content and can be approximately linear over material-specific calibration ranges [27,28,29]. Without a calibration specific to Trebgast sandstone, the MI values used here are therefore treated only as a proxy for relative spatial moisture distribution. Panico et al. [19] also stated that correlating MW readings with the amount of moisture is difficult. More information on principle and application are found in Orr et al. [30] and Sass & Heil [26].

2.4 Data preparation and processing

Given the large number of ERT datasets (16 profiles × 12 months = 192 models per year), the data required summarisation and reduction. An initial review showed that the overall pattern of resistance distribution remained broadly consistent across years. To capture representative spatial variability, we therefore focused on datasets from 2022 and 2023. Temporal variability was represented by selecting eight months for which high-quality data were available: January, April, July, and November 2022, and February, May, September, and December 2023. We used the Python package pyGIMLi to generate an individual 2D inversion model for each monthly survey. Prior to combining the monthly models, the inverted resistivity values were converted to electrical conductivity. Because electrical conductivity varies with temperature [31,32], all models were normalized to a reference temperature of 20 °C. The correction was derived from laboratory measurements of fully saturated Trebgast sandstone. A detailed description of the calculation procedure and derivation is provided in Appendix A. For each profile, the eight temperature-corrected conductivity models were combined using inverse-RMS weights ($w_i = 1/RMS_i$), giving less influence to models with higher inversion misfit (Appendix B). The RMS-weighted conductivity models were then transformed into an EC-derived relative moisture proxy ranging from 0 to 100%. To ensure comparability across all analyzed Trebgast sandstone profiles, a global logarithmic min–max normalization was applied. The normalized values represent a common relative scale for evaluating spatial moisture patterns and do not show absolute water content. The calculation is provided in Appendix C.

Complete handheld microwave datasets from both the R1M (0–3 cm) and PM (0–25 cm) sensors were available for the same eight selected measurement campaigns. Because the microwave response is temperature dependent, all raw measurements were corrected to a common reference temperature of 20 °C. The correction was derived from laboratory measurements of fully saturated Trebgast sandstone. Following temperature correction, the values from the eight selected measurement campaigns were arithmetically averaged at each measurement position. The resulting mean values were then transformed into a relative moisture proxy ranging from 0 to 100% using global min–max normalization, applied separately to the R1M and PM datasets. For each sensor, the normalization range was defined jointly from the mean ROCK and HOUSE values across all four wall orientations. As with conductivity, the normalized values therefore provide a relative measure of moisture variation within the investigated walls and do not show absolute water content. The complete calculation procedure is presented in Appendices D–E–F.

3. Results

3.1 Comparison between different stone faces

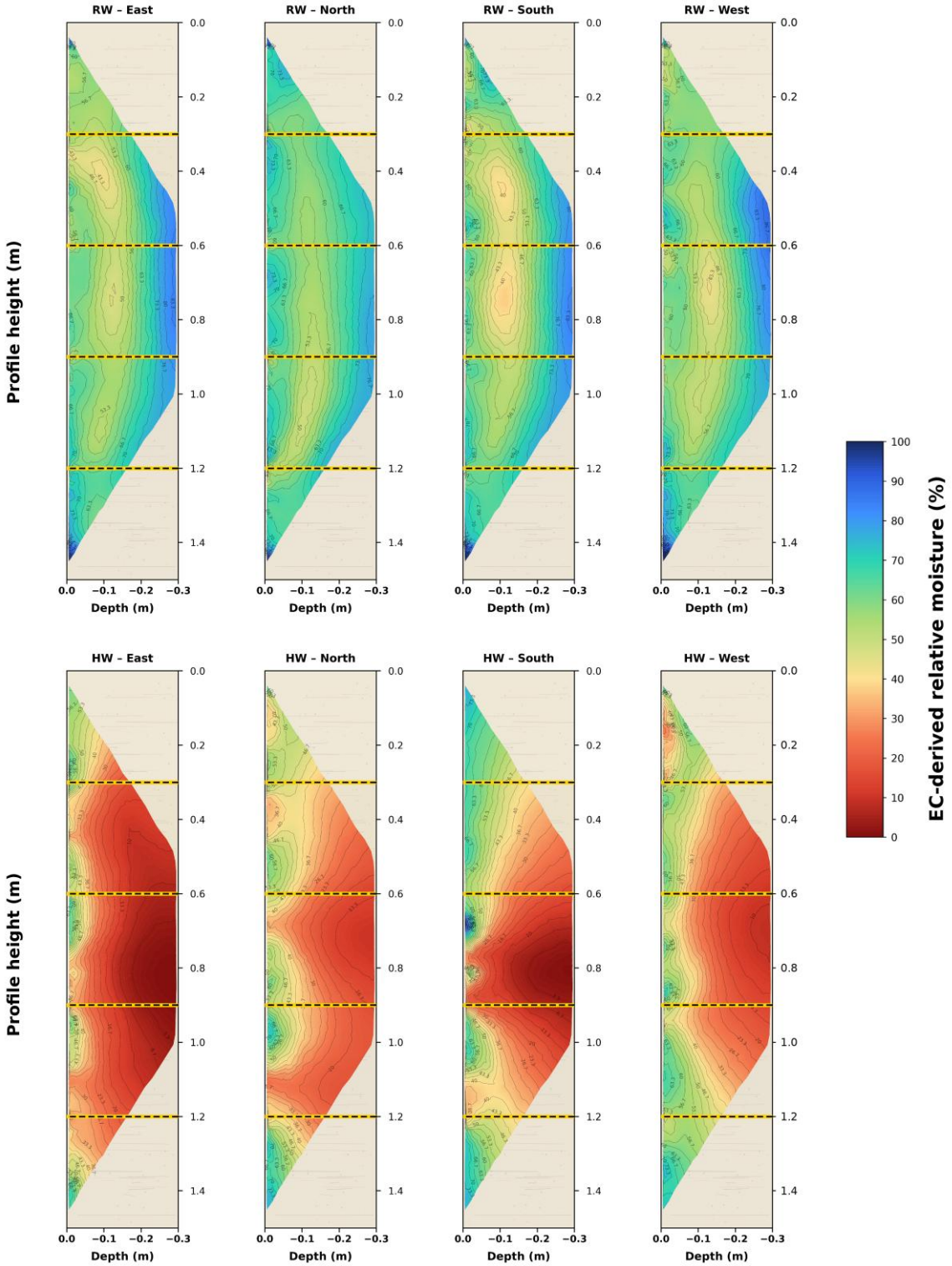


Fig. 3: EC-derived relative moisture in Trebgast sandstone for the ROCK (RW, upper row) and HOUSE (HW, lower row) in the four wall orientations. Each panel shows the RMS-weighted mean electrical conductivity corrected to 20 °C and converted by global logarithmic min–max normalization to a common 0–100% scale. The external wall surface is at 0 m depth and the inner side at −0.30 m; dashed horizontal lines indicate the interfaces between stone blocks: joints in ROCK and mortar planes in HOUSE.

Figure 3 reveals a distinct contrast between the two structures across all four wall orientations. Relative moisture is consistently higher in the ROCK profiles, with the highest values generally occurring toward the inner side of the wall. In contrast, the HOUSE profiles are characterized by lower values at greater depth, while relatively higher moisture occurs mainly near the external surface and locally along individual block boundaries. This difference is attributed to

the contrasting wall structures, with sand backfilling in ROCK and an air cavity in HOUSE. Although some variation is evident among the different orientations, these differences are less pronounced than the overall contrast between ROCK and HOUSE. The wettest orientations are West and North for ROCK, and South and West for HOUSE. In both structures, a wetter zone is also visible near the lower end of the profiles, particularly in ROCK, which is interpreted as an effect of capillary rise from the base.

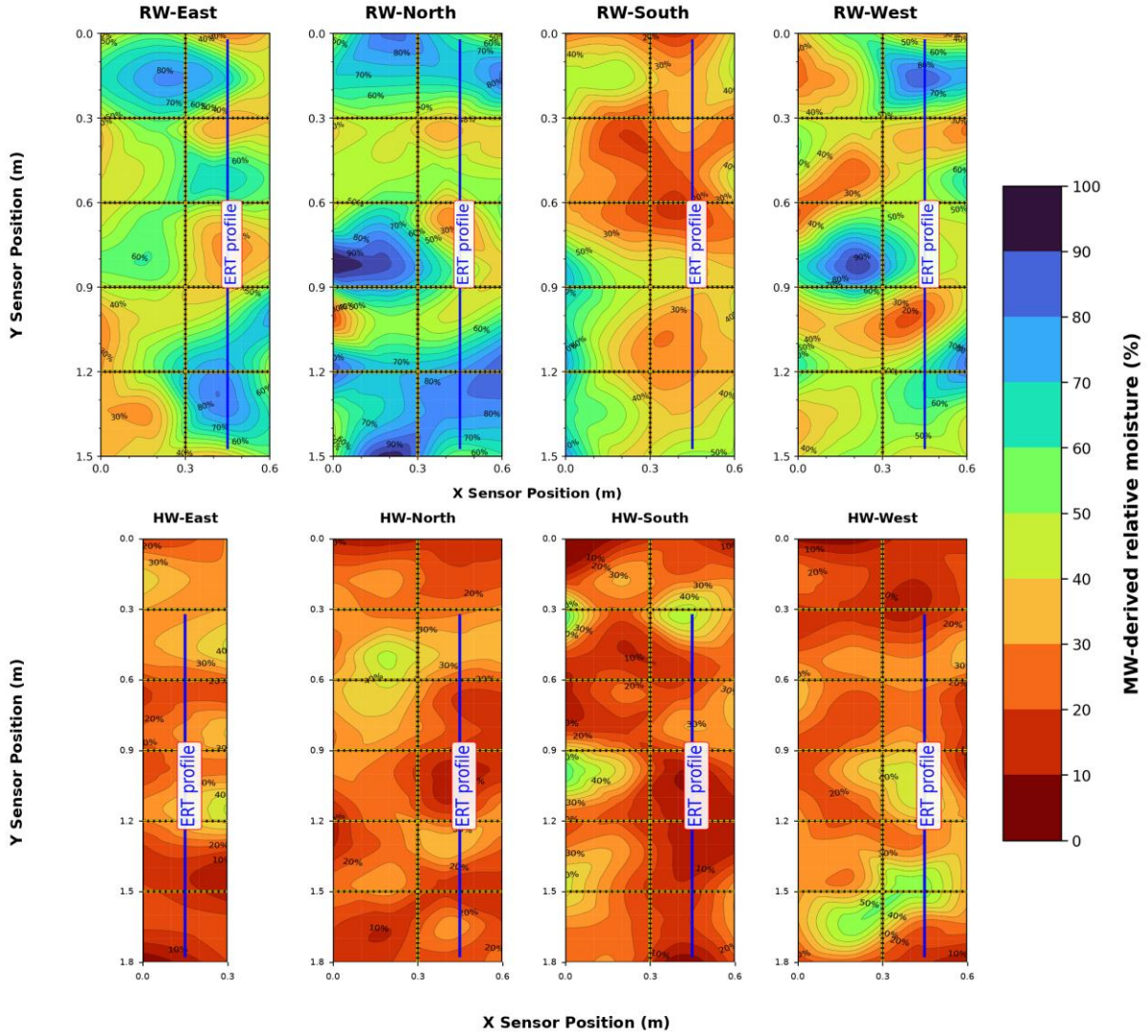


Fig. 4-1: MW-derived relative moisture in Trebgast sandstone for the ROCK (RW, upper row) and HOUSE (HW, lower row) in the four wall orientations. Each panel shows the arithmetic mean of eight R1M measurements (0–3 cm penetration depth) after correction to 20 °C and conversion by sensor-specific global min–max normalization to a common 0–100% relative scale. Dashed lines indicate the interfaces between stone blocks: joints in ROCK and mortar planes in HOUSE; the blue vertical line indicates the ERT profile position.

The MW-derived moisture distribution (Figure 4-1) demonstrates a pronounced difference in near-surface moisture between the two structures. ROCK generally exhibits substantially higher and more spatially heterogeneous relative moisture values than HOUSE. Among the ROCK orientations, the north wall shows the most extensive high-moisture zones, with values locally exceeding 80–90% in the middle and lower sections, while distinct wet areas are also present on the west and east walls. In contrast, the south wall is comparatively dry, with values predominantly around 20–40%. The HOUSE walls are generally characterized by lower relative moisture values, mostly within the 10–40% range, with only localized zones of intermediate moisture on individual blocks. Although some orientation-related variability is

evident, it is less pronounced than the overall difference between the uncovered, sand-filled ROCK and the roofed, ventilated HOUSE.

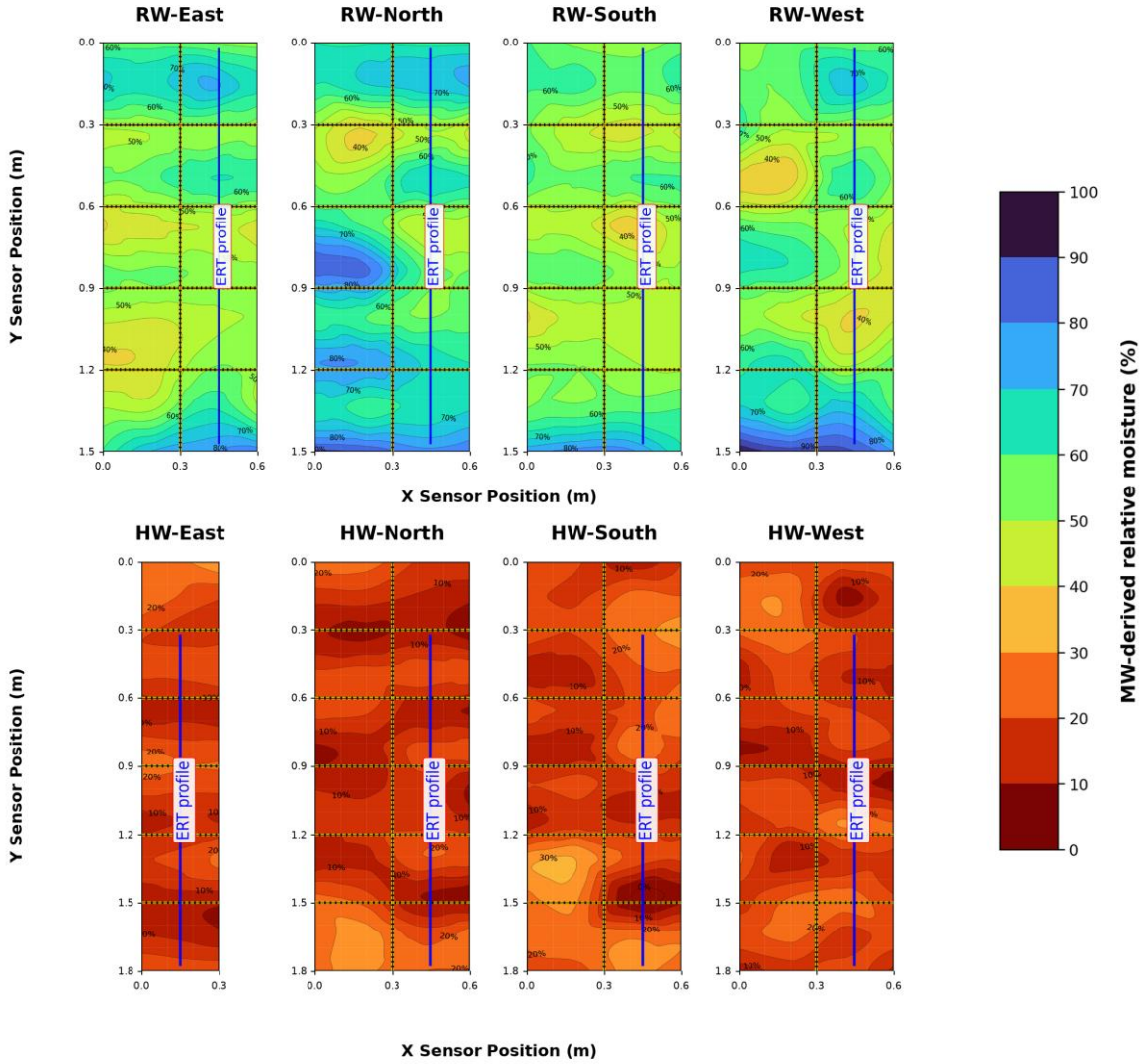


Fig. 4-2: MW-derived relative moisture in Trebgast sandstone for the ROCK (RW, upper row) and HOUSE (HW, lower row) in the four wall orientations. Each panel shows the arithmetic mean of eight PM measurements (0–25 cm penetration depth) after correction to 20 °C and conversion by sensor-specific global min–max normalization to a common 0–100% relative scale. Dashed lines indicate the interfaces between stone blocks: joints in ROCK and mortar planes in HOUSE; the blue vertical line indicates the ERT profile position.

Figure 4-2 presents the deeper microwave response and shows a stronger contrast between ROCK and HOUSE. ROCK is characterized predominantly by intermediate to high relative moisture values, typically around 40–80%, with the most extensive high-value zones on the north- and west-facing walls. Values above 80% occur mainly in the lower parts of these walls, whereas the south-facing wall is more uniform and generally lower. Elevated values near the base are visible in all four ROCK orientations. In at least 20 of the 40 ROCK blocks, the lower half of the block has a higher relative moisture value than the upper half. HOUSE remains in the lower part of the PM-specific relative scale, generally around 5–25%, with only localized zones approaching 20–30%. Compared with the R1M maps, the PM patterns are spatially smoother, consistent with the larger measurement volume of the deeper sensor. Because R1M and PM were normalized independently, their percentages describe relative spatial variation within each sensor dataset and cannot be compared directly as absolute moisture levels.

3.2 Surface vertical moisture profiles (including joints/mortar planes)

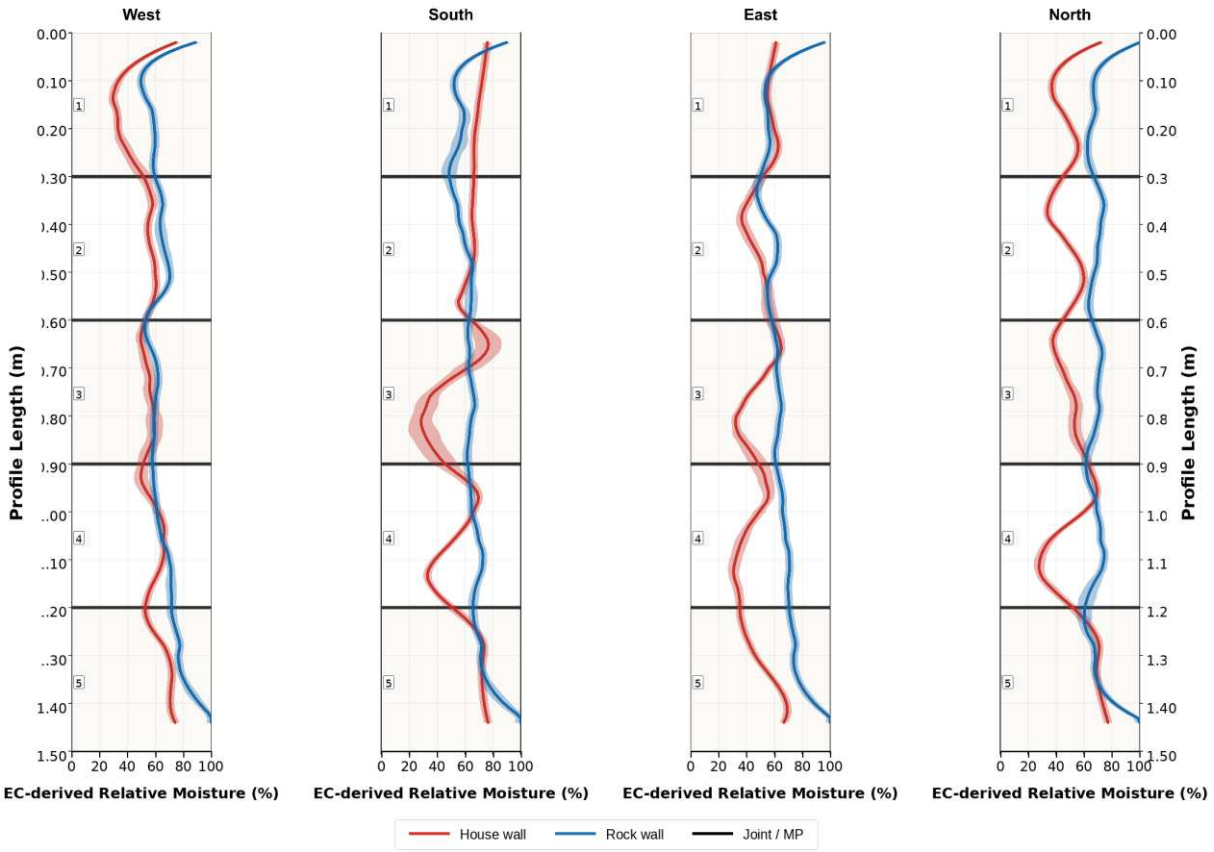


Fig. 5: Surface EC-derived relative moisture profiles at the wall surface for the HOUSE and ROCK walls in the west, south, east, and north orientations. Horizontal black lines indicate block interfaces: joints in ROCK and mortar planes in HOUSE.

Figure 5 summarizes the surface EC-derived relative moisture along the vertical profiles of ROCK and HOUSE for all four orientations. ROCK generally shows higher surface moisture values than HOUSE, with the strongest separation observed on the east- and north-facing walls. Greater overlap between the two structures occurs along parts of the west and south profiles. Within ROCK, several orientations show pronounced local maxima in the upper and lower sections of the walls, whereas the HOUSE profiles are generally lower and less variable. Localized changes in the profiles occur near some joints or mortar planes, but these features are not consistently reproduced across interfaces or orientations. In general, the results indicate that differences between the two structures are more pronounced than any systematic moisture response associated with individual block boundaries.

3.3 Depth-dependent vertical moisture profiles

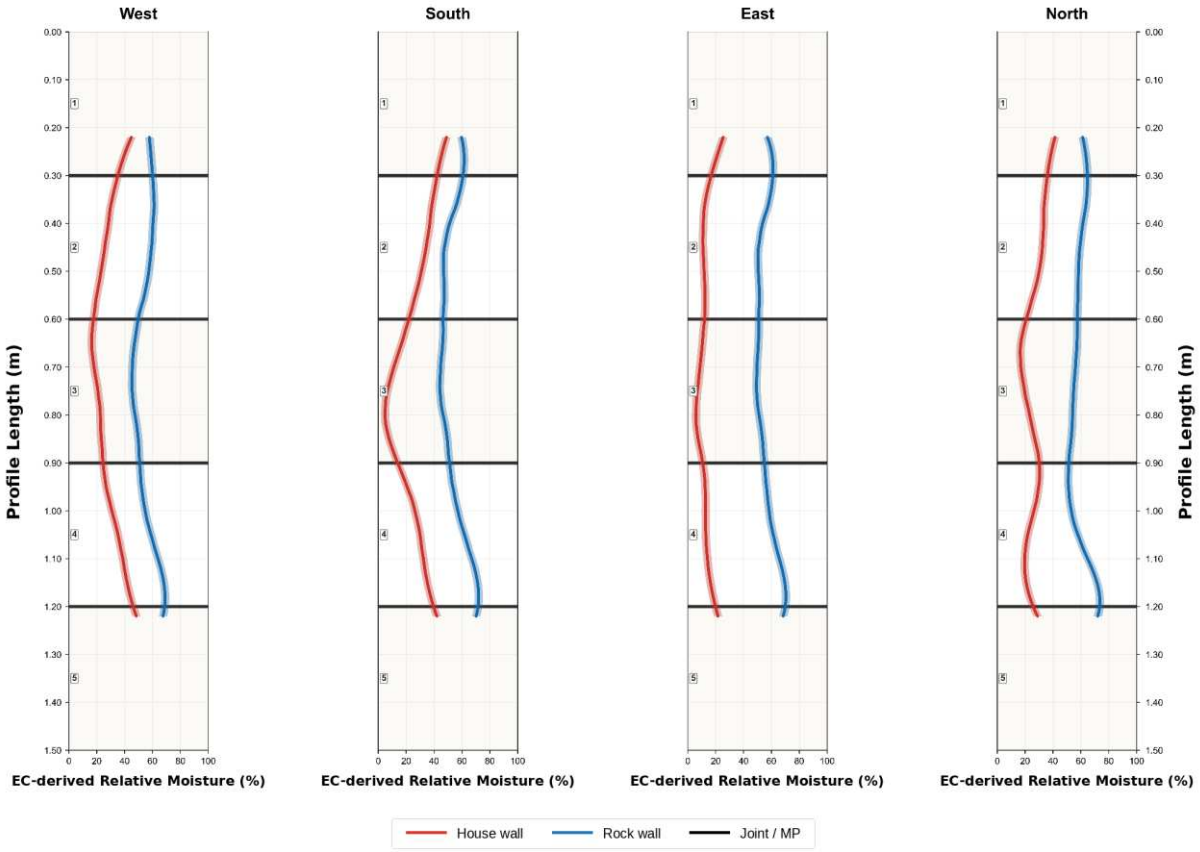


Fig. 6-1: EC-derived vertical relative moisture profiles at 15 cm wall depth for the HOUSE and ROCK walls in the four wall orientations. Horizontal black lines indicate block interfaces: joints in ROCK and mortar planes in HOUSE.

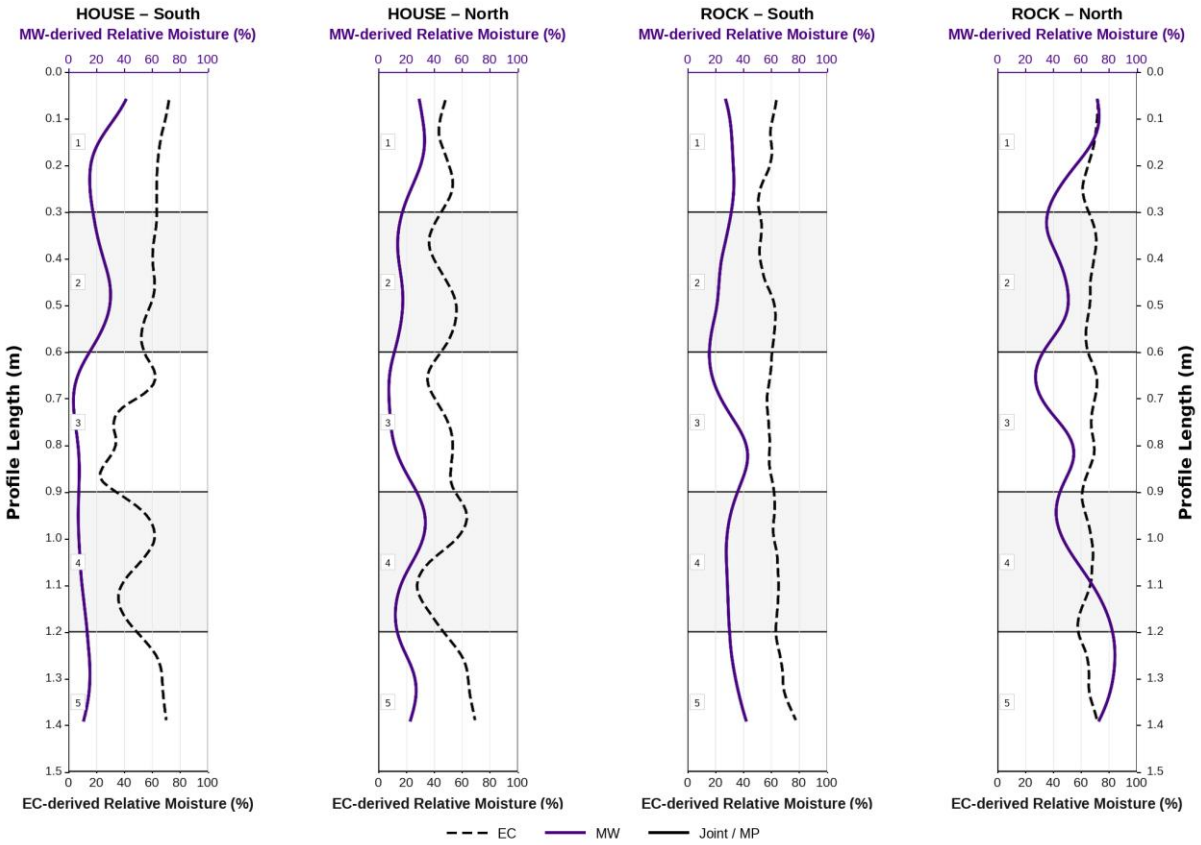


Fig. 6-2: Shallow-zone comparison of vertical relative moisture profiles for HOUSE (left two panels) and ROCK (right two panels), comparing ERT-derived EC values at 3 cm wall depth with MW(R1M) values (0–3 cm) for the south and north orientations. Horizontal black lines indicate block interfaces: mortar planes in HOUSE and joints in ROCK.

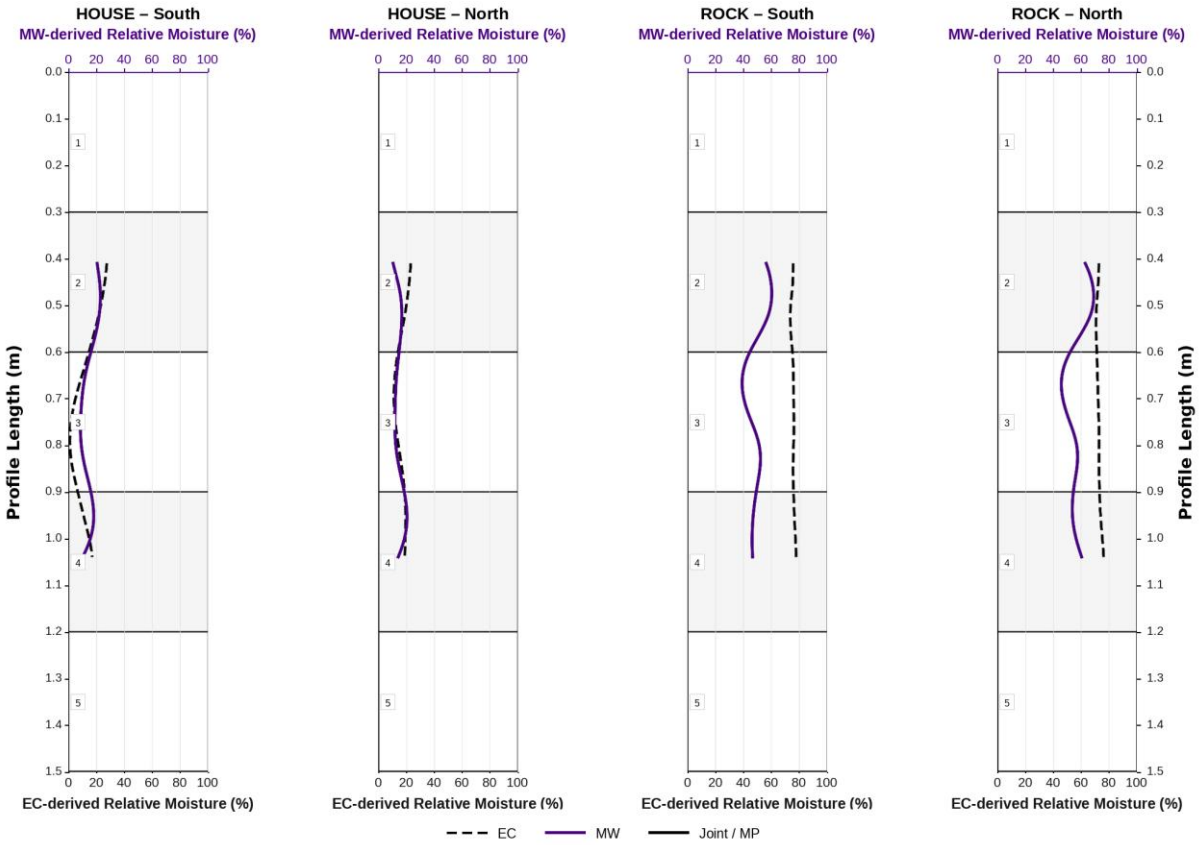


Fig. 6-3: Deep-zone comparison of vertical relative moisture profiles for HOUSE (left two panels) and ROCK (right two panels), comparing ERT-derived EC values at 25 cm wall depth with MW(PM) values (0–25 cm) for the south and north orientations. Horizontal black lines indicate block interfaces: mortar planes in HOUSE and joints in ROCK.

Figure 6-1 shows the EC-derived vertical profiles at 15 cm wall depth, which are comparatively smooth across the four orientations. Figures 6-2 and 6-3 directly compare EC and MW profile forms at shallow and deep sampling depths, respectively. For these comparisons, MW values were extracted along the transect spatially coincident with the ERT profile position, indicated by the blue vertical line in the MW maps (Figs. 4-1 and 4-2). At 3 cm (Fig. 6-2), the closest profile-shape correspondence occurs for HOUSE North and locally for ROCK North, whereas larger differences occur for HOUSE South and ROCK South. At 25 cm (Fig. 6-3), HOUSE North and HOUSE South show similar broad vertical trends in ERT and MW(PM), while correspondence is weaker for ROCK. Because the EC- and MW-derived datasets were normalized independently, these comparisons concern profile shape and the vertical position of relative maxima and minima rather than equality of the numerical moisture-proxy values.

3.4 Comparison between electrical conductivity and microwave sensing

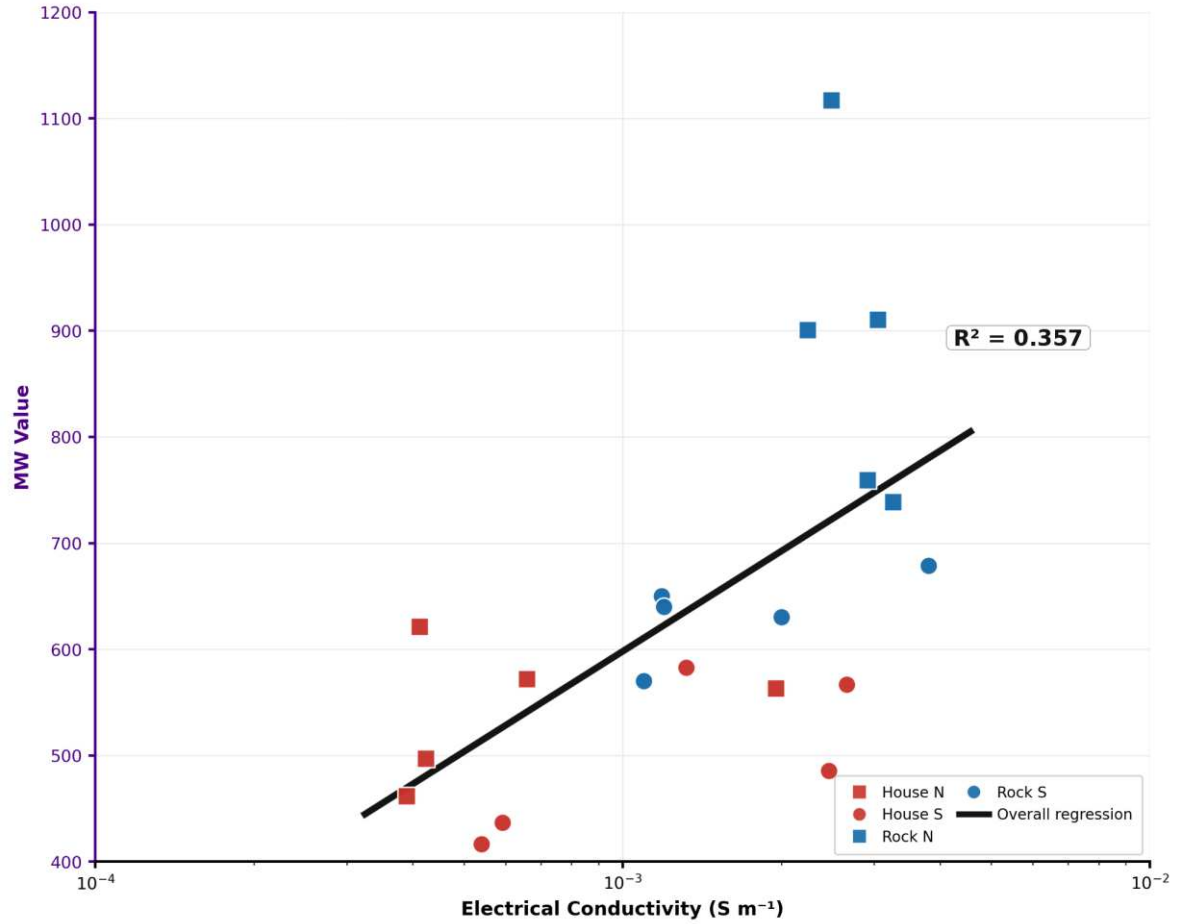


Fig. 7-1: Block-wise comparison of electrical conductivity (EC) and microwave R1M measurements at shallow sampling depth (0–3 cm), pooling the north and south faces of HOUSE and ROCK. Each point represents the mean EC and MW value of one stone block (B1–B5). Colour identifies structure (HOUSE: red; ROCK: blue), while marker shape identifies orientation (North: squares; South: circles). The black line is a single linear regression fitted to all 20 pooled block means (R^2 = 0.357).

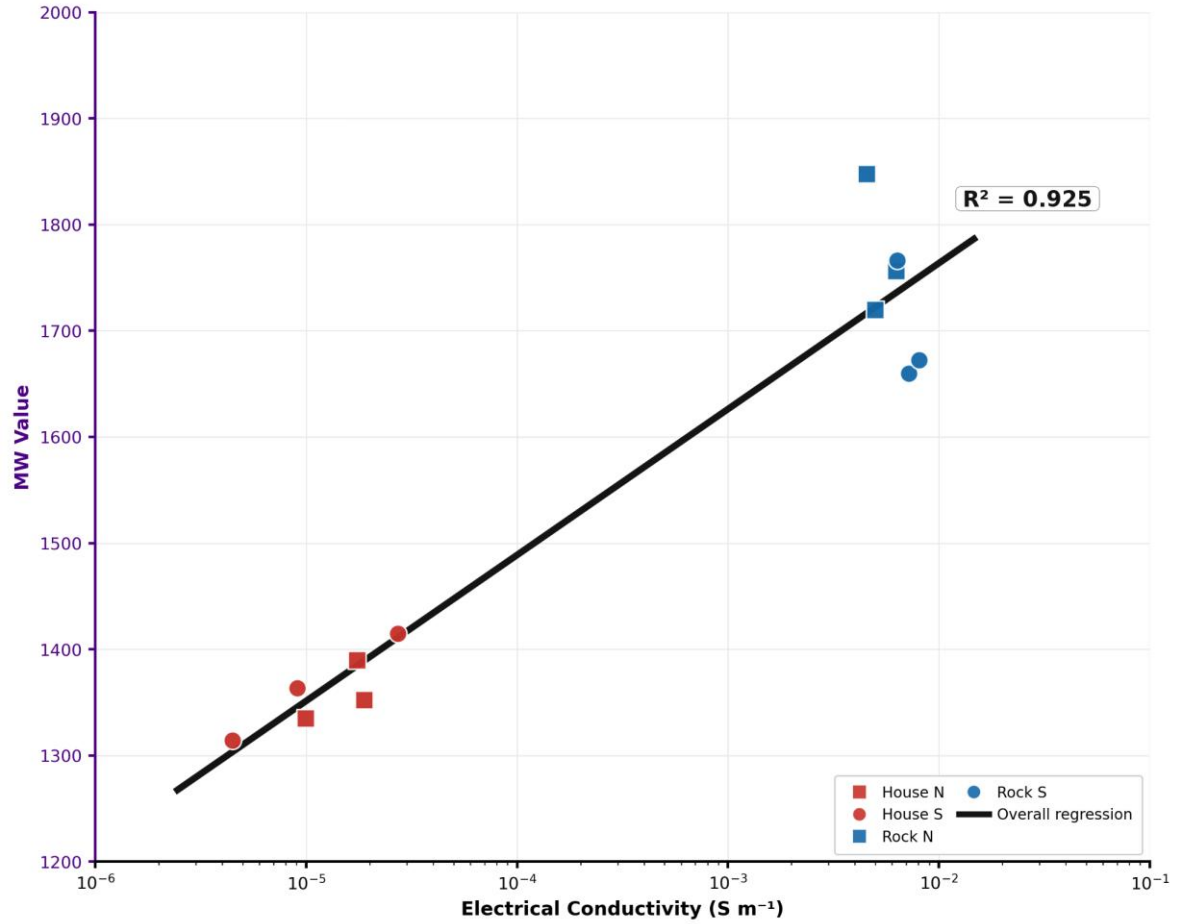


Fig. 7-2: Block-wise comparison of electrical conductivity (EC) and microwave PM measurements at deep sampling depth (0–25 cm), pooling the north and south faces of HOUSE and ROCK. Each point represents the mean EC and MW value of one available stone block (B2–B4). Colour identifies structure (HOUSE: red; ROCK: blue), while marker shape identifies orientation (North: squares; South: circles). The black line is a single linear regression fitted to all 12 pooled block means (R^2 = 0.925).

Figures 7-1 and 7-2 examine the overall covariance between block-mean EC and MW responses after pooling the north and south faces of both structures. At shallow depth, the 20 pooled block means show a positive but only moderate relationship (R^2 = 0.357), with substantial scatter remaining among blocks and wall groups. At the deeper sampling depth, the 12 pooled block means show a very strong overall relationship (R^2 = 0.925). In this deep comparison, HOUSE occupies the lower EC and MW range, whereas ROCK occupies the higher range, so the regression primarily captures the first-order structural contrast between the drier HOUSE and wetter ROCK. Thus, the two methods agree much more strongly on the broad deep moisture contrast than on shallow block-to-block variability.

4. Discussion

The first evaluations of spatial moisture distribution from the UBT test walls indicate that the strongest observed moisture differences are related to the structural configuration of the test walls and the ensuing hydrological boundary conditions. Wall orientation, vertical position, measurement depth and sensing method modify this first-order pattern. The clearest and most consistent result is the higher relative moisture of ROCK compared with HOUSE in the same Trebgast sandstone (Figs. 3, 4-1 and 4-2). This contrast is most plausibly related to the different hydrological boundary conditions of the two structures. ROCK is uncovered, contains a sand-filled interior and is in basal contact with the surrounding sand, whereas HOUSE is

roofed, drained away from the structure and ventilated internally. While the EC-derived proxy was normalized globally across all analyzed Trebgast sandstone profiles, the MW-derived proxy was normalized separately for each sensor after pooling measurements from ROCK and HOUSE. The resulting 0-100% values therefore describe relative spatial moisture differences within each method and should not be interpreted as absolute water content. Future field-based calibration is needed to translate these relative indices into physically interpretable moisture values.

The depth-dependent patterns are consistent with the contrasting boundary conditions of the two structures. In ROCK, relatively high moisture commonly extends toward the inner side of the wall, whereas HOUSE generally shows lower values toward its ventilated interior (Fig. 3; Figs. 6-1–6-3). Locally high moisture in the uppermost ROCK stones is consistent with direct infiltration from the uncovered top into the stonework while the persistent increase toward the inner side of many ROCK profiles is consistent with rear-side moisture supply from the wet sand backfill. The long-term spatial averages do not quantify the relative fluxes of these two pathways, but their different spatial signatures allow them to be distinguished conceptually. Event-resolved observations during rainfall will be required to test this separation and to determine how rapidly top infiltration and backfill-derived moisture propagate through the wall.

Basal moisture enrichment is consistent with capillary rise, particularly in ROCK; the evidence is less conclusive for HOUSE. Enhanced moisture occurs near the base in the 2D EC-derived maps and in the deeper MW(PM) patterns (Figs. 3 and 4-2), and several vertical profiles show maxima in the lowest stone or a decrease in relative moisture upward from the base. This repeated basal enhancement is consistent with upward capillary supply from the moist sand of the basin fill. The interpretation is especially plausible for ROCK because the lower stones are in direct contact with the surrounding sand, while HOUSE shows a weaker and less persistent basal signal, consistent with its slightly raised foundation and drainage configuration. Studies of historic masonry likewise show that rising damp depends strongly on water availability, wall depth, evaporation conditions and construction details [33,34,35]. The UBT patterns are therefore compatible with basal capillary supply, especially in ROCK, but do not independently quantify upward water flux.

Wall orientation influences the moisture distribution, but its effect is secondary to the ROCK–HOUSE contrast and varies with depth and measurement method. Meteorological forcing is strongly directional: wind-driven rain is concentrated in the western sector, whereas solar radiation is concentrated toward the south (Fig. 2). In ROCK, the north- and west-facing walls are generally the wettest and the south-facing wall is comparatively dry, giving an approximate sequence N > W > E > S. This is consistent with patterns of WDR input and radiative drying. HOUSE shows a less stable and weaker orientation signal; across the spatial averages, west and south are generally among the wetter faces, while north and east are lower or intermediate, but the ordering changes between methods and depths. One plausible reason is that the roof, drainage and raised basal contact suppress the additional top and bottom water sources that amplify moisture contrasts in ROCK. HOUSE may therefore express a comparatively 'purer' façade-exposure signal dominated by WDR and drying, but at a much lower overall moisture level. Investigations by Blocken and Carmeliet [36] and Blocken and Carmeliet [37] support the assumption that the impact of driving rain on a façade is not determined solely by its overall direction of exposure, but also significantly by local wind flow, building geometry, corner turbulence and the position on the façade. Furthermore, Janssen et al. [38] show that the directional dependence of the driving rain coefficient may be of secondary importance under certain model assumptions.

The influence of joints and mortar planes is more localized. The surface EC profiles show short-scale changes close to some block interfaces, but no moisture anomaly occurs systematically at every joint or mortar plane (Fig. 5). The deeper microwave maps provide an additional pattern in ROCK: at least 20 of the 40 blocks show higher moisture in their lower

half. This distribution may be consistent with gravity-driven downward water redistribution and local blockage effects of horizontal contacts. Strong and variable impact of the interface between building stones and mortar on water movement was also emphasized by Zhou et al. [39]. Evidence is scarcer for unmortared joints; the presented spatial averages point at dry horizontal joints often acting as barriers but there is no uniform joint-controlled moisture pattern across the walls. Previous studies have shown that mortar and joints can play different hydrological roles depending on material properties and exposure conditions [30,40].

The comparison between ERT and handheld microwave measurements shows that correspondence depends strongly on spatial scale and sampling depth. Both methods distinguish the generally wetter ROCK from the drier HOUSE. At the profile scale, some vertical patterns correspond well, especially HOUSE North at shallow depth and both HOUSE orientations at deeper sampling depth (Figs. 6-2 and 6-3), whereas other profiles differ. The pooled block comparisons sharpen this picture. At shallow depth, the overall north–south relationship is only moderate ($R^2 = 0.357$; Fig. 7-1), indicating that local block-to-block variation is captured differently by EC and R1M. At the deeper sampling depth, the pooled relationship is very strong ($R^2 = 0.925$; Fig. 7-2), but the regression is largely controlled by the clear separation between HOUSE at lower EC/MW values and ROCK at higher values. The high R^2 therefore demonstrates strong agreement in the first-order structural moisture contrast rather than a direct one-to-one calibration between the two sensing methods at block scale. A likely reason for the remaining local mismatch is that the two methods do not sample equivalent geometries. ERT values are obtained from an inverted 2D sensitivity field generated by current flow between electrodes; each model cell is influenced by a spatially distributed volume around the electrode line, and inversion regularization smooths sharp local contrasts. By contrast, a handheld MW reading is a local surface measurement that integrates dielectric response over a finite footprint and a depth-dependent sensing volume. In particular, MW(PM) integrates information from approximately 0–25 cm rather than representing a discrete value exactly at 25 cm, whereas the ERT comparison extracts model values at a nominal depth. Surface contact, roughness and the different weighting of near-surface versus deeper material can therefore shift individual block means even when both methods respond consistently to the broad wet–dry structure. The two approaches are consequently complementary for spatial pattern detection but should not be treated as interchangeable moisture scales without a geometry-aware field calibration. This scale-dependent interpretation provides a practical basis for selecting ERT and microwave sensing as complementary rather than interchangeable methods in non-destructive surveys of historic stone masonry.

Calibration remains the main methodological limitation. Laboratory calibration was carried out for both EC and MW, but the laboratory response ranges did not fully encompass the values recorded in the field. Applying the laboratory relationships directly to field data would, in parts of the walls, produce implausibly high or low inferred moisture values. A comparable laboratory–field mismatch was reported by Sass [28], where field microwave and electrical measurements extended beyond the corresponding laboratory calibration ranges. For this reason, relative moisture indices were calculated from the minimum and maximum values of the temperature-corrected field datasets which provide a robust basis for comparing spatial wetness patterns. The need for material- and condition-specific calibration (and its difficulties) is well established for moisture measurements in porous building materials [2,16,27].

We plan to address this limitation through future on-site calibration using controlled wetting experiments. This could involve the use of automated spraying systems, such as sprinklers, combined with simultaneous EC and MW measurements while the walls are progressively wetted until a stable maximum sensor response is reached. This maximum response, together with minimum values recorded during prolonged dry periods, could then be used to establish a field-based min–max calibration for each measurement method. The UBT test walls are particularly well suited for this purpose because controlled water application can be carried out without the conservation and access restrictions typically associated with heritage structures.

The observed ROCK–HOUSE contrast in the same Trebgast sandstone illustrates why moisture patterns in historic masonry should not be interpreted from stone type or façade orientation alone. The combined structural influence of roof and drainage configuration, basal contact, rear-side water availability and ventilation may substantially influence the location of relatively wet zones. For conservation-oriented monitoring, it therefore supports documenting construction and exposure conditions alongside sensor observations before attributing local moisture anomalies to a particular water pathway. In the heritage-hydrology framework of Sass & Viles [1], such differences can be understood in terms of water inputs, transfers, storage and outputs. The test walls constrain the spatial expression of these interacting components, but do not measure their individual fluxes. Accordingly, anomalously high near-surface moisture at a heritage site should prompt assessment of drainage, ground contact, internal ventilation and potential rear-side supply before it is attributed solely to façade exposure.

The fundamentally different measurement geometries of ERT and MW matter when selecting methods and interpreting individual anomalies in historic stonework. Neither relative proxy should be regarded as absolute water content. This finding is consistent with the documented difficulties of quantitative microwave moisture assessment in masonry [19] and underlines the value of combining complementary measurement geometries.

Based on the findings we suggest a specific interpretation sequence for future surveys of historic stone masonry: (1) document accessible construction and exposure information, including cover, drainage, ground contact and possible rear-side moisture supply; (2) evaluate whether a measured anomaly is persistent across complementary sensing volumes before relating it to a proposed moisture pathway. The applicability to historic masonry with salts, undocumented repairs, mixed materials or different wall geometries remains to be tested.

The experimental walls do not replicate the full material and construction heterogeneity of historic buildings. Spatial analyses in this paper primarily concern Trebgast sandstone, and their relative moisture indices depend on the normalization and material response applied here. The eight selected campaigns were aggregated to characterize spatial patterns; they do not establish seasonal moisture dynamics, which is examined as part of the broader long-term monitoring programme. Moreover, the configurations of ROCK and HOUSE differ in several properties simultaneously, and water fluxes from the top, rear and base were not independently measured. Transfer of the present interpretation to any particular heritage site will therefore require additional material-specific calibration, attention to survey geometry and appropriate field validation. In particular, soluble salts and heterogeneous mortar or repair materials may affect electrical and dielectric responses independently of water content.

The UBT experiment demonstrates the potential of full-scale, documented test walls as reference platforms for built-heritage moisture research. The experiment separates a robust structural contrast from the more variable effects of orientation and sensing geometry. Such reference measurements may help frame non-destructive monitoring strategies for historic stone masonry, although direct conservation decisions require validation under site-specific conditions.

Acknowledgements

We thank Manfred Fischer for carrying out most of the measurements in 2022/2023 and Andrew Mitchell for support and calibration work.

References

[1] Sass, O. & Viles, H. (2022): Heritage hydrology: a conceptual framework for understanding water fluxes and storage in built and rock-hewn heritage. Heritage Science 10: 66. https://doi.org/10.1186/s40494-022-00693-7.

[2] Sandrolini, F. & Franzoni, E. (2006): An operative protocol for reliable measurements of moisture in porous materials of ancient buildings. Building and Environment 41(10): 1372–1380. https://doi.org/10.1016/j.buildenv.2005.05.023.

[3] McGreevy, J.P. & Whalley, W.B. (1985): Rock Moisture Content and Frost Weathering under Natural and Experimental Conditions: A Comparative Discussion. Arctic and Alpine Research 17(3): 337–346. https://doi.org/10.1080/00040851.1985.12004040.

[4] Matsuoka, N. & Murton, J.B. (2008): Frost weathering: Recent advances and future directions. Permafrost and Periglacial Processes 19(2): 195–210. https://doi.org/10.1002/ppp.620.

[5] Mitchell, A. & Sass, O. (2024): Rock weathering: The effects of varying rock moisture on controlled weathering cycles in low porosity limestone. Geomorphology 457: 109149. https://doi.org/10.1016/j.geomorph.2024.109149.

[6] Goudie, A. & Viles, H. (1997): Salt Weathering Hazards. Wiley, Chichester.

[7] Doehne, E. (2002): Salt weathering: A selective review. Geological Society, London, Special Publications 205(1): 51–64. https://doi.org/10.1144/GSL.SP.2002.205.01.05.

[8] Eppes, M.-C. & Keanini, R. (2017): Mechanical weathering and rock erosion by climate-dependent subcritical cracking. Reviews of Geophysics 55: 470–508. https://doi.org/10.1002/2017RG000557.

[9] Gorbushina, A.A. (2007): Life on the rocks. Environmental Microbiology 9(7): 1613–1631. https://doi.org/10.1111/j.1462-2920.2007.01301.x.

[10] Viles, H.A. & Cutler, N.A. (2012): Global environmental change and the biology of heritage structures. Global Change Biology 18(8): 2406–2418. https://doi.org/10.1111/j.1365-2486.2012.02713.x.

[11] McCabe, S., Smith, B.J., McAlister, J.J., Gomez-Heras, M., McAllister, D., Warke, P.A., Curran, J.M. & Basheer, P.A.M. (2013): Changing climate, changing process: Implications for salt transportation and weathering within building sandstones in the UK. Environmental Earth Sciences 69(4): 1225–1235. https://doi.org/10.1007/s12665-013-2278-2.

[12] Smith, B.J., Gomez-Heras, M. & McCabe, S. (2008): Understanding the decay of stone-built cultural heritage. Progress in Physical Geography 32(4): 439–461. https://doi.org/10.1177/0309133308098119.

[13] Coletti, C. (2024): Climate Change Threats to Stone Cultural Heritage: State of the Art of Quantitative Damage Functions and New Challenges for a Sustainable Future. Heritage 7: 3276–3290. https://doi.org/10.3390/heritage7060154.

[14] Gomez-Heras, M. & McCabe, S. (2015): Weathering of stone-built heritage: A lens through which to read the Anthropocene. Anthropocene 11: 1–13. https://doi.org/10.1016/j.ancene.2015.12.003.

[15] Sass, O. (2005): Rock moisture measurements: techniques, results, and implications for weathering. Earth Surface Processes and Landforms 30(3): 359–374. https://doi.org/10.1002/esp.1214.

[16] Viles, H., Zhang, H. & Orr, S. (2022): A Comparative Evaluation of Methods to Monitor Moisture in Historic Porous Masonry Materials. Historic England Research Report Series 2/2022. ISSN 2059-4453.

[17] Weiss, T. & Sass, O. (2022): The challenge of measuring rock moisture–a laboratory experiment using eight types of sensors. Geomorphology 416: 108430. https://doi.org/10.1016/j.geomorph.2022.108430.

[18] Guolo, E., Falchi, L., Cimino, D., Balliana, E., Peron, F., Zendri, E. (2025): Investigation of capillary rise in brick masonry models under controlled conditions. Construction and Building Materials 483: 141793.

[19] Panico, S., Herrera-Avellanosa, D., Troi, A. (2023): Monitoring rising damp in solid masonry walls: An experimental comparison of five different methods. Journal of Building Engineering 75: 106999.

[20] De Groeve, M., Kale, E., Godts, S., Orr, S.A. & De Kock, T. (2024): Impact of vertical greening on urban microclimate and historic building materials: A meta-analysis. Building and Environment 253: 111365. https://doi.org/10.1016/j.buildenv.2024.111365.

[21] Agliata, R., Greco, R. & Mollo, L. (2018): Moisture Measurements in Heritage Masonries: A Review of Current Techniques. Materials Evaluation 76(11): 1468–1477.

[22] Tucker, M. & Fosbury, R. (2021): Iron Minerals in Bath Stone (Great Oolite, Middle Jurassic, UK): Pyrite, Goethite and Glauconite, their Spectra and Origins. Journal of the Bath Geological Society 39: 48–52.

[23] Reda, I. & Andreas, A. (2004): Solar position algorithm for solar radiation applications. Solar Energy 76(5): 577–589. https://doi.org/10.1016/j.solener.2003.12.003.

[24] Sass, O. & Viles, H.A. (2010): Wetting and drying of masonry walls: 2D-resistivity monitoring of driving rain experiments on historic stonework in Oxford, UK. Journal of Applied Geophysics 70(1): 72–83. https://doi.org/10.1016/j.jappgeo.2009.11.006.

[25] Rode, M., Sass, O., Kellerer-Pirklbauer, A., Schnepfleitner, H. & Gitschthaler, C. (2020): Permafrost distribution and conditions at the headwalls of two receding glaciers (Schladming and Hallstatt glaciers) in the Dachstein Massif, Northern Calcareous Alps, Austria. The Cryosphere 14: 1173–1186. https://doi.org/10.5194/tc-14-1173-2020.

[26] Sass, O. & Heil, S. (2024): The role of moisture and salt distribution in the weathering of the medieval cave town of Uplistsikhe, Georgia. Heritage Science 12: 197. https://doi.org/10.1186/s40494-024-01310-5.

[27] Piuzzi, E., Pittella, E., Pisa, S., Cataldo, A., De Benedetto, E. & Cannazza, G. (2018): Microwave reflectometric methodologies for water content estimation in stone-made Cultural Heritage materials. Measurement 118: 275–281. https://doi.org/10.1016/j.measurement.2017.05.069.

[28] Sass, O. (2022): Investigating rock moisture at a sandstone massif in the Saxonian Switzerland climbing area. Journal of Geomorphology 1(1): 25–41. https://doi.org/10.1127/jgeomorphology/2022/0711.

[29] D'Alvia, L., Pittella, E., Rizzuto, E., Piuzzi, E. & Del Prete, Z. (2022): A portable low-cost reflectometric setup for moisture measurement in cultural heritage masonry unit. Measurement 189: 110438. https://doi.org/10.1016/j.measurement.2021.110438.

[30] Orr, S.A., Fusade, L., Young, M., Stelfox, D., Leslie, A., Curran, J. & Viles, H. (2020): Moisture monitoring of stone masonry: A comparison of microwave and radar on a granite wall and a sandstone tower. Journal of Cultural Heritage 41: 61–73. https://doi.org/10.1016/j.culher.2019.07.011.

[31] Hayley, K., Bentley, L.R., Gharibi, M. & Nightingale, M. (2007): Low temperature dependence of electrical resistivity: Implications for near surface geophysical monitoring. Geophysical Research Letters 34: L18402. https://doi.org/10.1029/2007GL031124.

[32] Hayley, K., Bentley, L.R. & Pidlisecky, A. (2010): Compensating for temperature variations in time-lapse electrical resistivity difference imaging. Geophysics 75(4): WA51–WA59. https://doi.org/10.1190/1.3478208.

[33] Franzoni, E., Bandini, S. & Graziani, G. (2014): Rising moisture, salts and electrokinetic effects in ancient masonries: From laboratory testing to on-site monitoring. Journal of Cultural Heritage 15(2): 112–120. https://doi.org/10.1016/j.culher.2013.03.003.

[34] Falchi, L., Slanzi, D., Balliana, E., Driussi, G. & Zendri, E. (2018): Rising damp in historical buildings: A Venetian perspective. Building and Environment 131: 117–127. https://doi.org/10.1016/j.buildenv.2018.01.004.

[35] Franzoni, E., Berk, B., Bassi, M. & Marrone, C. (2023): An integrated approach to the monitoring of rising damp in historic brick masonry. Construction and Building Materials 370: 130631. https://doi.org/10.1016/j.conbuildmat.2023.130631.

[36] Blocken, B. J. E., & Carmeliet, J. E. (2004): A review of wind-driven rain research in building science. Journal of Wind Engineering and Industrial Aerodynamics, 92(13): 1079–1130.

[37] Blocken, B. J. E., & Carmeliet, J. E. (2006): The influence of the wind-blocking effect by a building on its wind-driven rain exposure. Journal of Wind Engineering and Industrial Aerodynamics, 94(2): 101–127.

[38] Janssen, H., Blocken, B. J. E., Roels, S., & Carmeliet, J. E. (2007): Wind-driven rain as a boundary condition for HAM simulations: Analysis of simplified modelling approaches. Building and Environment, 42(4): 1555–1567.

[39] Zhou, X., Desmarais, G., Vontobel, P., Carmeliet, J., & Derome, D. (2020): Masonry brick–cement mortar interface resistance to water transport determined with neutron radiography and numerical modeling. Journal of Building Physics, 44(3): 251–271. https://doi.org/10.1177/1744259120908967

[40] Michette, M., Viles, H., Vlachou, C. & Angus, I. (2021): In Situ, Non-Destructive Testing for Evaluating the Role of Pointing Mortar in Preventive Conservation Strategies: A Case-Study on Reigate Stone at the Wardrobe Tower, Tower of London. Minerals 11(4): 345. https://doi.org/10.3390/min11040345.

Authorship contribution statement

Oliver Sass: Conceptualization, Funding acquisition, Supervision, Investigation, Methodology, Writing – original draft, Writing – review & editing.

Alireza Madani: Investigation, Formal analysis, Visualization, Software, Methodology, Writing – original draft, Writing – review & editing.

Appendices

Appendix A: Temperature correction of ERT data using the fully saturated laboratory relationship

Let the inverted electrical resistivity at model cell (x, z), measured at stone temperature T, be denoted by $\rho_{\mathrm{raw}}(x,z,T)$. The corresponding raw electrical conductivity was calculated as:

$$\sigma_{\mathrm{raw}}(x,z,T) = \frac{1}{\rho_{\mathrm{raw}}(x,z,T)} \tag{1}$$

Laboratory measurements of fully saturated Trebgast sandstone were represented by the following linear conductivity-temperature relationship, where T is in °C and conductivity is in S m⁻¹:

$$\sigma_{\mathrm{sat}}(T) = a_{\mathrm{sat}}T + b_{\mathrm{sat}} = 7.91 \times 10^{-5}T + 1.99 \times 10^{-3} \tag{2}$$

$$\sigma_{\mathrm{sat}}(20) = 3.572 \times 10^{-3}\ \mathrm{S\,m^{-1}} \tag{3}$$

For each model cell, the measured conductivity was corrected to 20 °C using the ratio between the saturated-state conductivity at the reference temperature and at the survey temperature:

$$\sigma_{20}(x,z) = \frac{\sigma_{\mathrm{raw}}(x,z,T)}{1 + a_{\mathrm{sat}}(T-20)} \tag{4}$$

Here, $\sigma_{20}(x,z)$ is the conductivity of model cell (x, z) corrected to 20°C, while $\sigma_{\mathrm{raw}}(x,z,T)$ is the conductivity calculated from the 2D-inverted resistivity data at stone temperature T. a_{sat} is the slope derived from fully saturated Trebgast sandstone. The fully saturated relationship was used solely as the material-specific basis for the temperature correction; no assumption of full saturation was made for the field data.

Appendix B: RMS-based quality weighting of ERT models

For each profile, the temperature-corrected conductivity models from the eight selected ERT surveys were combined using the following weighted mean:

$$\overline{\sigma}_{20,w}(x,z) = \frac{\sum_{i=1}^{n} w_i\, \sigma_{20,i}(x,z)}{\sum_{i=1}^{n} w_i}, \qquad n = 8 \tag{5}$$

Here, $\sigma_{20,i}(x, z)$ is the temperature-corrected conductivity at model cell (x, z) for survey i. The weight was set to $w_i = 1/RMS_i$, where RMS_i is the reported inversion misfit of that survey. Thus, models with higher RMS contribute less to the mean and models with lower RMS contribute more to the mean:

$$\mathrm{w_i} = 1 \,/\, \mathrm{RMS_i} \tag{6}$$

Appendix C: Conversion of RMS-weighted conductivity to an EC-derived relative moisture proxy

Let $\overline{\sigma}_{20,w}(x,z)$ denote the RMS-weighted electrical conductivity corrected to 20 °C. To place all analysed profiles on a common scale while retaining contrasts across the wide conductivity range, all electrical conductivity values were transformed to relative moisture using a global logarithmic min–max normalization:

$$\mathrm{RM_{EC}}(x,z) = 100 \times [\ln(\overline{\sigma}_{20,w}(x,z)) - \ln(\overline{\sigma}_{20,w,min}(x,z))] \,/\, [\ln(\overline{\sigma}_{20,w,max}(x,z)) - \ln(\overline{\sigma}_{20,w,min}(x,z))] \tag{7}$$

Here, $\mathrm{RM_{EC}}(x,z)$ is the EC-derived relative moisture for model cell (x,z); $\overline{\sigma}_{20,w}(x,z)$ is the RMS-weighted mean electrical conductivity at that cell, corrected to 20 °C; $\overline{\sigma}_{20,w,min}(x,z)$ is the minimum of all $\overline{\sigma}_{20,w}(x,z)$ values (2.330756 × 10^{-6} S m^{-1}); and $\overline{\sigma}_{20,w,max}(x,z)$ is the corresponding maximum (9.372761 × 10^{-2} S m^{-1}). The proxy was constrained to 0–100% and represents relative spatial moisture variation rather than absolute water content.

Appendix D: Temperature correction of handheld microwave data

Microwave readings vary slightly with stone temperature. To make measurements from different campaigns directly comparable, every field value was converted to 20 °C as reference temperature. For each sensor, the temperature response measured in the laboratory on fully saturated Trebgast sandstone was described by:

$$MW_{sat,R1M}(T) = -4.014\ T + 1010.548 \tag{8}$$

$$MW_{sat,PM}(T) = -1.150\ T + 2212.624 \tag{9}$$

The correction is a simple ratio: the field reading is multiplied by the laboratory response at 20 °C and divided by the laboratory response at the temperature measured during the survey:

$$MW_{raw,20} = MW_{raw,}\ (T_f) \times MW_{sat,20} \,/\, MW_{sat}\ (T_f) \tag{10}$$

Here, $MW_{raw,}\ (T_f)$ is the field reading at the measured profile temperature T_f, $MW_{sat}\ (T_f)$ and $MW_{sat,20}$ are the laboratory responses of the same sensor at T_f and 20 °C, and $MW_{raw,20}$ is the temperature-corrected value. The correction was applied independently to every reading. The saturated laboratory curves were used only to quantify temperature sensitivity; the field stone was not assumed to be saturated.

Appendix E: Calculation of mean handheld microwave values

At each measurement position, the eight temperature-corrected values were combined using a simple arithmetic mean:

$$\overline{MW}_{\mathrm{raw,20}} = (1 / 8)\ \Sigma_{i=1}^{8}\ MW_{raw,20,\,i} \tag{11}$$

Appendix F: Conversion to a MW-derived relative moisture

For each sensor type, the mean values were rescaled to a common 0–100% range using min–max normalization:

$$RM_{MW} = 100 \times (\overline{MW}_{raw,20} - \overline{MW}_{raw,20,min}) / (\overline{MW}_{raw,20,max} - \overline{MW}_{raw,20,min}) \quad (12)$$

$\overline{MW}_{raw,20,min}$ and $\overline{MW}_{raw,20,max}$ are the lowest and highest mean values observed for that sensor after pooling ROCK and HOUSE measurements from all four wall orientations. Normalization was performed separately for R1M and PM because their response ranges and penetration depths differ. Thus, 0% and 100% indicate the lowest and highest values in the respective dataset.